EQUATORIAL WAVES

A. V. Fedorov and J. N. Brown, Yale University, New Haven, CT, USA

Introduction

It has been long recognized that the tropical thermocline (the sharp boundary between warm and deeper cold waters) provides a wave guide for several types of large-scale ocean waves. The existence of this wave guide is due to two key factors. First, the mean ocean vertical stratification in the tropics is perhaps greater than anywhere else in the ocean (Figures 1 and 2), which facilitates wave propagation. Second, since the Coriolis parameter vanishes exactly at 0° of latitude, the equator works as a natural boundary, suggesting an analogy between coastally trapped and equatorial waves.

The most well-known examples of equatorial waves are eastward propagating Kelvin waves and westward propagating Rossby waves. These waves are usually observed as disturbances that either raise or lower the equatorial thermocline. These thermocline disturbances are mirrored by small anomalies in sea-level elevation, which offer a practical method for tracking these waves from space.

For some time the theory of equatorial waves, based on the shallow-water equations, remained a theoretical curiosity and an interesting application for Hermite functions. The first direct measurements of equatorial Kelvin waves in the 1960s and 1970s served as a rough confirmation of the theory. By the 1980s, scientists came to realize that the equatorial waves, crucial in the response of the tropical ocean

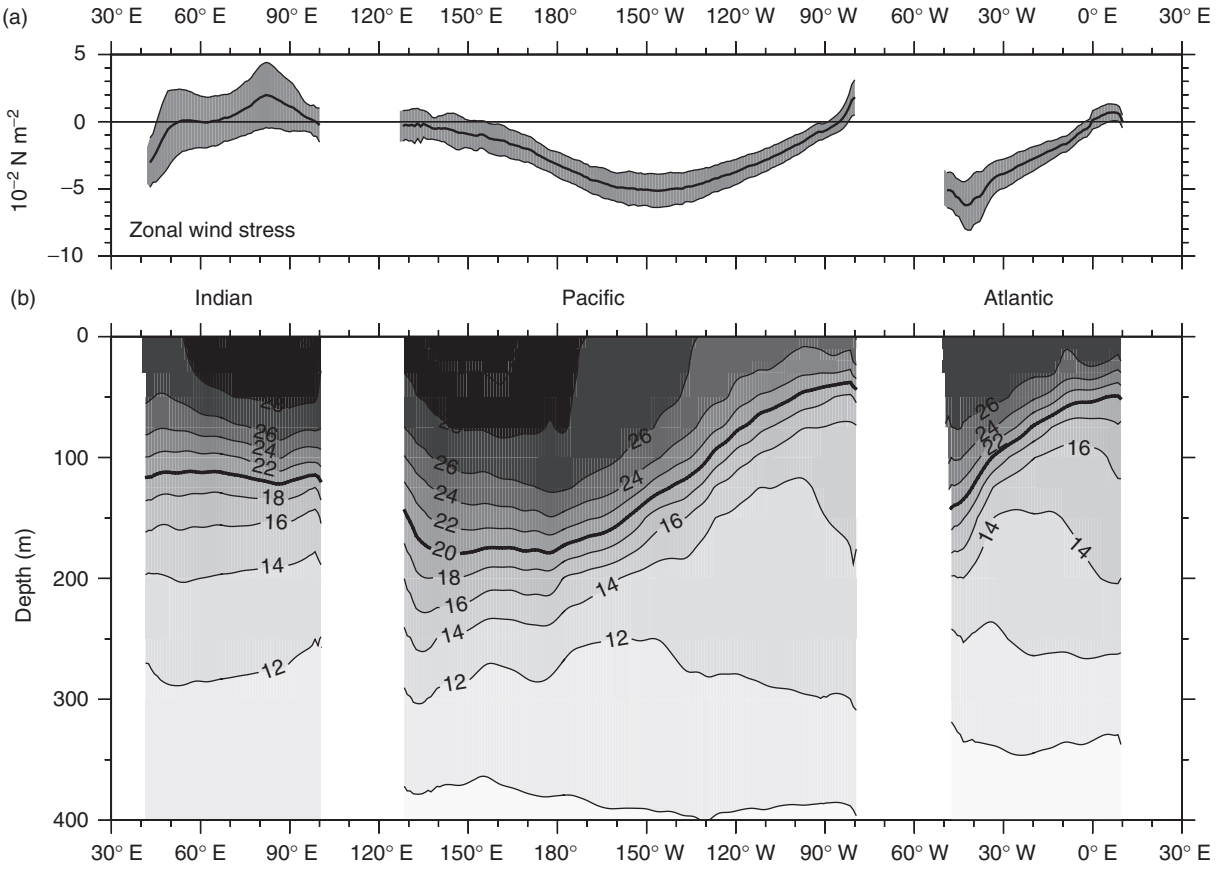

Figure 1 The thermal structure of the upper ocean along the equator: (a) the zonal wind stress along the equator; shading indicates the standard deviation of the annual cycle. (b) Ocean temperature along the equator as a function of depth and longitude. The east–west slope of the thermocline in the Pacific and the Atlantic is maintained by the easterly winds. (b) From Kessler (2005).

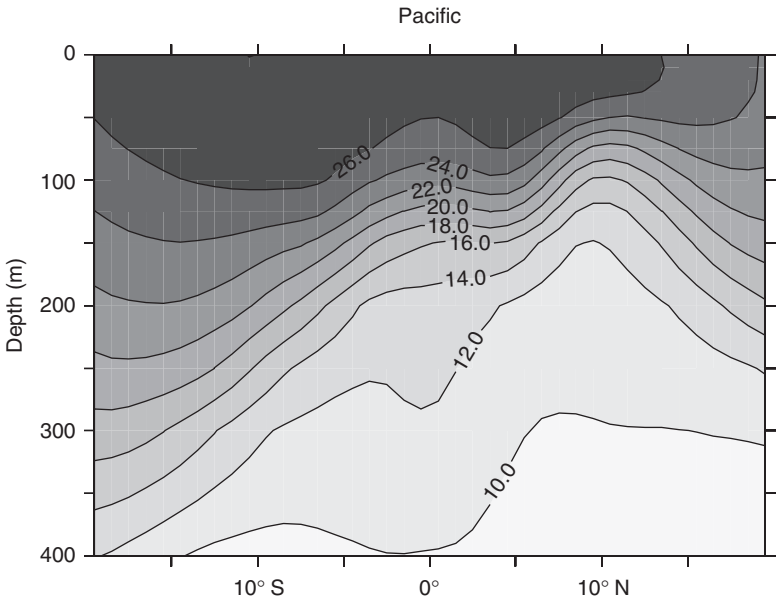

Figure 2 Ocean temperature as a function of depth and latitude in the middle of the Pacific basin (at 140° W). The thermocline is particularly sharp in the vicinity of the equator. Note that the scaling of the horizontal axis is different from that in **Figure 1**. Temperature data are from Levitus S and Boyer T (1994) *World Ocean Atlas 1994, Vol. 4: Temperature NOAA Atlas NESDIS4.* Washington, DC: US Government Printing Office.

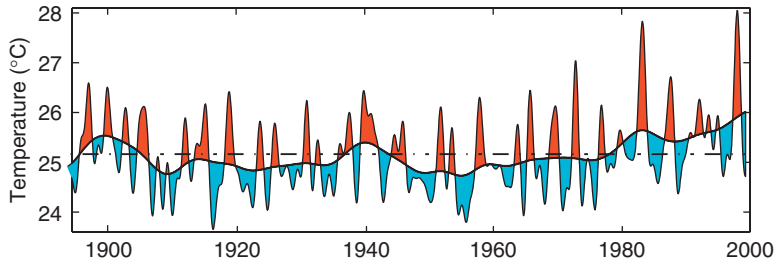

Figure 3 Interannual variations in sea surface temperatures (SSTs) in the eastern equatorial Pacific shown on the background of decadal changes (in °C). The annual cycle and high-frequency variations are removed from the data. El Niño conditions correspond to warmer temperatures. Note El Niño events of 1982 and 1997, the strongest in the instrumental record. From Fedorov AV and Philander SG (2000) Is El Niño changing? *Science* 288: 1997–2002.

to varying wind forcing, are one of the key factors in explaining ENSO – the El Niño-Southern Oscillation phenomenon.

El Niño, and its complement La Niña, have physical manifestations in the sea surface temperature (SST) of the eastern equatorial Pacific (**Figure 3**). These climate phenomena cause a gradual horizontal redistribution of warm surface water along the equator: strong zonal winds during La Niña years pile up the warm water in the west, causing the thermocline to slope downward to the west and exposing cold water to the surface in the east (**Figure 4(b)**). During an El Niño, weakened zonal winds permit the warm water to flow back eastward so that the thermocline becomes more horizontal, inducing strong warm anomalies in the SST (**Figure 4(a)**).

The ocean adjustment associated with these changes crucially depends on the existence of equatorial waves, especially Kelvin and Rossby waves, as they can alter the depth of the tropical thermocline. This article gives a brief summary of the theory behind equatorial waves, the available observations of those waves, and their role in ENSO dynamics. For a detailed description of El Niño phenomenology the reader is referred to other relevant papers in this encyclopedia El Niño Southern Oscillation (ENSO)El Niño Southern Oscillation (ENSO) Modelsand Pacific Ocean Equatorial Currents.

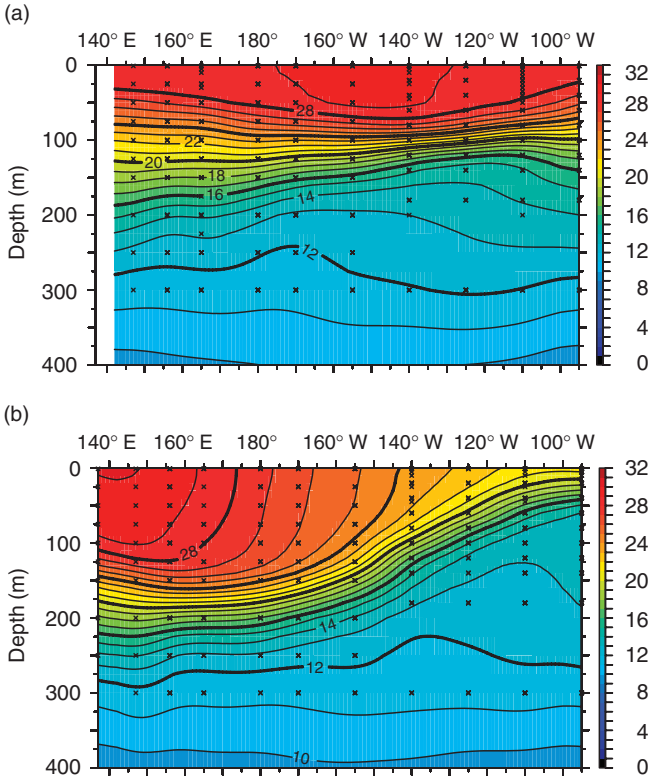

Figure 4 Temperatures (°C) as a function of depth along the equator at the peaks of (a) El Niño (Jan. 1998) and (b) La Niña (Dec. 1999). From the TAO data; see McPhaden MJ (1999) Genesis and evolution of the 1997–98 El Niño. *Science* 283: 950–954.

It is significant that ENSO is characterized by a spectral peak at the period of 3–5 years. The timescales associated with the low-order (and most important dynamically) equatorial waves are much shorter than this period. For instance, it takes only 2–3 months for a Kelvin wave to cross the Pacific basin, and less than 8 months for a first-mode Rossby wave. Because of such scale separation, the properties of the ocean response to wind perturbations strongly depend on the character of the imposed forcing. It is, therefore, necessary to distinguish the following.

1. Free equatorial waves which arise as solutions of unforced equations of motion (e.g., free Kelvin and Rossby waves),
2. Equatorial waves forced by brief wind perturbations (of the order of a few weeks). In effect, these waves become free waves as soon as the wind perturbation has ended,
3. Equatorial wave-like anomalies forced by slowly varying periodic or quasi-periodic winds reflecting ocean adjustment on interannual timescales. Even though these anomalies can be represented mathematically as a superposition of continuously forced Kelvin and Rossby waves of different modes, the properties of the superposition (such as the propagation speed) can be rather different from the properties of free waves.

The Shallow-Water Equations

Equatorial wave dynamics are easily understood from simple models based on the $1\frac{1}{2}$-layer shallow-water equations. This approximation assumes that a shallow layer of relatively warm (and less dense) water overlies a much deeper layer of cold water. The two layers are separated by a sharp thermocline (Figure 5), and it is assumed that there is no motion in the deep layer. The idea is to approximate the thermal (and density) structure of the ocean displayed in Figures 1 and 2 in the simplest form possible.

The momentum and continuity equations, usually referred to as the reduced-gravity shallow-water equations on the β-plane, are

$$u_t + g'h_x - \beta y v = \tau^x/\rho D - \alpha_s u \qquad [1]$$

$$v_t + g'h_y + \beta y u = \tau^y/\rho D - \alpha_s v \qquad [2]$$

$$h_t + H(u_x + v_y) = -\alpha_s h \qquad [3]$$

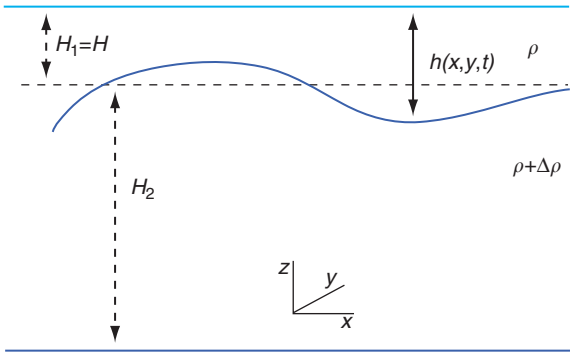

Figure 5 A sketch of the $1\frac{1}{2}$-layer shallow-water system with the rigid-lid approximation. $H_1/H_2 \ll 1$. The mean depth of the thermocline is H. The x-axis is directed to the east along the equator. The y-axis is directed toward the North Pole. The mean east–west thermocline slope along the equator is neglected.

These equations have been linearized, and perturbations with respect to the mean state are considered. Variations in the mean east–west slope of the thermocline and mean zonal currents are neglected. The notations are conventional (some are shown in Figure 5), with u, v denoting the ocean zonal and meridional currents, H the mean depth of the thermocline, h thermocline depth anomalies, τ^x and τ^y the zonal and meridional components of the wind stress, ρ mean water density, $\Delta\rho$ the difference between the density of the upper (warm) layer and the deep lower layer, $g' = g\Delta\rho/\rho$ the reduced gravity. D is the nominal depth characterizing the effect of wind on the thermocline (frequently it is assumed that $D = H$). The subscripts t, x, and y indicate the respective derivatives.

The system includes simple Rayleigh friction in the momentum equations and a simple linear parametrization of water entrainment at the base of the mixed layer in the continuity equation (terms proportional to α_s). Some typical values for the equatorial Pacific are $\Delta\rho/\rho = 0.006$; $H = 120\,\text{m}$ (see Figure 1); $D = 80\,\text{m}$. The rigid-lid approximation is assumed (i.e., to a first approximation the ocean surface is flat). However, after computing h, one can calculate small changes in the implied elevation of the free surface as $\eta = -h\Delta\rho/\rho$. It is this connection that allows us to estimate changes in the thermocline depth from satellite measurements by measuring sea-level height.

The boundary conditions for the equations are no zonal flow ($u = 0$) at the eastern and western boundaries and vanishing meridional flow far away from the equator. The former boundary conditions are sometimes modified by decomposing u into different wave components and introducing reflection coefficients (smaller than unity) to account for a partial reflection of waves from the boundaries.

It is apparent that the $1\frac{1}{2}$-layer approach leaves in the system only the first baroclinic mode and eliminates barotropic motion (the first baroclinic mode describes a flow that with different velocities in two layers, barotropic flow does not depend on the vertical coordinate). This approximation filters out higher-order baroclinic modes with more elaborate vertical structure. For instance, the equatorial undercurrent (EUC) is absent in this model. Observations and numerical calculations show that to represent the full vertical structure of the currents and ocean response to winds correctly, both the first- and second-baroclinic modes are necessary. Nevertheless, the shallow-water equations within the $1\frac{1}{2}$-layer approximation remain very successful and are used broadly in the famous Cane-Zebiak model of ENSO and its numerous modifications.

For many applications, the shallow-water equations are further simplified to filter out short waves: in the long-wave approximation the second momentum equation (eqn [2]) is replaced with a simple geostrophic balance:

$$g'h_y + \beta y u = 0 \qquad [4]$$

The boundary condition at the western boundary is then replaced with the no-net flow requirement $\left(\int u dy = 0\right)$.

It is noteworthy that the shallow-water equations can also approximate the mean state of the tropical ocean (if used as the full equations for mean variables, rather than perturbations from the mean state). In that case the main dynamic balance along the equator is that between the mean trade winds and the mean (climatological) slope of the thermocline (damping neglected)

$$g'h_x \sim \tau^x/\rho D \qquad [5]$$

This balance implies the east–west difference in the thermocline depth along the equator of about 130 m in the Pacific consistent with Figure 1.

Free-Wave Solutions of the Shallow-Water Equations

First, we consider the shallow-water eqns [1]–[3] with no forcing and no dissipation. The equations have an infinite set of equatorially trapped solutions (with $v \to 0$ for $y \to \pm\infty$). These are free equatorial waves that propagate back and forth along the equator.

Kelvin Waves

Kelvin waves are a special case when the meridional velocity vanishes everywhere identically ($v = 0$) and eqns [1]–[3] reduce to

$$u_t + g'h_x = 0 \qquad [6]$$

$$g'h_y + \beta y u = 0 \qquad [7]$$

$$h_t + Hu_x = 0 \qquad [8]$$

Looking for wave solutions of [6]–[8] in the form

$$[u, v, h] = [\tilde{u}(y), \tilde{v}(y), \tilde{h}(y)]\mathrm{e}^{\mathrm{i}(kx-\omega t)} \qquad [9]$$

$$\tilde{v}(y) = 0; \quad \omega > 0 \qquad [10]$$

we obtain the dispersion relation for frequency ω and wave number k

$$\omega^2 = g'Hk^2 \qquad [11]$$

and a first-order ordinary differential equation for the meridional structure of h

$$\frac{\mathrm{d}\tilde{h}}{\mathrm{d}y} = -\frac{\beta k}{\omega} y\tilde{h} \qquad [12]$$

The only solution of [11] and [12] decaying for large y, called the Kelvin wave solution, is

$$h = h_0 \mathrm{e}^{-(\beta/2c)y^2}\mathrm{e}^{\mathrm{i}(kx-\omega t)} \qquad [13]$$

where the phase speed $c = (g'H)^{1/2}$ and $\omega = ck$ (h_0 is an arbitrary amplitude). Thus, Kelvin waves are eastward propagating ($\omega/k > 0$) and nondispersive. The second solution of [11] and [12], the one that propagates westward, would grow exponentially for large y and as such is disregarded.

Calculating the Kelvin wave phase speed from typical parameters used in the shallow-water model gives $c = 2.7\,\mathrm{m\,s^{-1}}$ which agrees well with the measurements. The meridional scale with which these solutions decay away from the equator is the equatorial Rossby radius of deformation defined as

$$L_R = (c/\beta)^{1/2} \qquad [14]$$

which is approximately 350 km in the Pacific Ocean, so that at 5° N or 5° S the wave amplitude reduces to 30% of that at the equator.

Rossby, Poincare, and Yanai Waves

Now let us look for the solutions that have nonzero meridional velocity v. Using the same representation as in [9] we obtain a single equation for $\tilde{v}(y)$:

$$\frac{\mathrm{d}^2\tilde{v}}{\mathrm{d}y^2} + \left(\frac{\omega^2}{c^2} - k^2 - \frac{\beta k}{\omega} - \frac{\beta^2}{c^2}y^2\right)\tilde{v} = 0 \qquad [15]$$

The solutions of [15] that decay far away from the equator exist only when an important constraint connecting its coefficients is satisfied:

$$\frac{\omega^2}{c^2} - k^2 - \frac{\beta k}{\omega} = (2n+1)\frac{\beta}{c} \qquad [16]$$

where $n = 0, 1, 2, 3, \ldots$. This constraint serves as a dispersion relation $\omega = \omega(k,n)$ for several different types of equatorial waves (see Figure 6), which include

1. Gravity-inertial or Poincare waves $n = 1, 2, 3, \ldots$
2. Rossby waves $n = 1, 2, 3, \ldots$
3. Rossby-gravity or Yanai wave $n = 0$
4. Kelvin wave $n = -1$.

These waves constitute a complete set and any solution of the unforced problem can be represented as a sum of those waves (note that the Kelvin wave is formally a solution of [15] and [16] with $v = 0$, $n = -1$).

Let us consider several important limits that will elucidate some properties of these waves. For high frequencies we can neglect $\beta k/\omega$ in [16] to obtain

$$\omega^2 = c^2k^2 + (2n+1)\beta c \qquad [17]$$

where $n = 1, 2, 3, \ldots$.

This is a dispersion relation for gravity-inertial waves, also called equatorially trapped Poincare waves. They propagate in either direction and are similar to gravity-inertial waves in mid-latitudes.

For low frequencies we can neglect ω^2/c^2 in [16] to obtain

$$\omega = -\frac{\beta k}{k^2 + (2n+1)\beta/c} \qquad [18]$$

with $n = 1, 2, 3, \ldots$. These are Rossby waves similar to their counterparts in mid-latitudes that critically depend on the β-effect. Their phase velocity (ω/k) is always westward ($\omega/k < 0$), but their group velocity $\partial\omega/\partial k$ can become eastward for high wave numbers.

The case $n = 0$ is a special case corresponding to the so-called mixed Rossby-gravity or Yanai wave. Careful consideration shows that when the phase velocity of those waves is eastward ($\omega/k > 0$), they behave like gravity-inertial waves and [17] is satisfied, but when the phase velocity is westward ($\omega/k < 0$), they behave like Rossby waves and expression [18] becomes more appropriate.

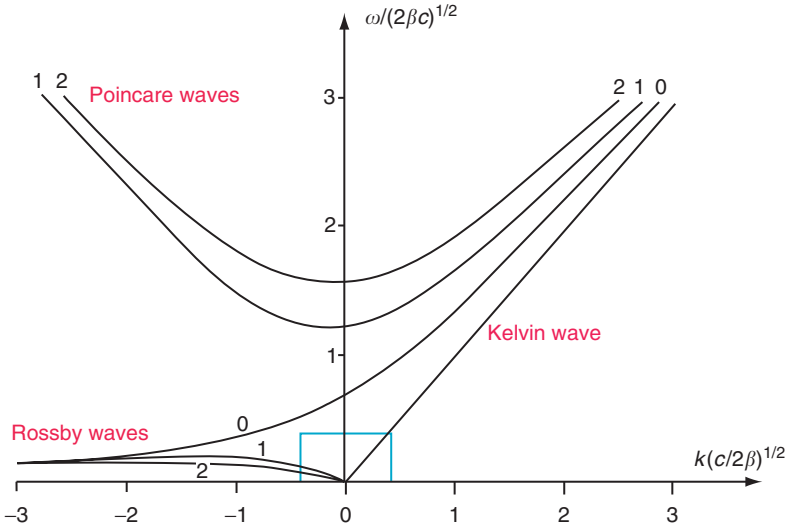

Figure 6 The dispersion relation for free equatorial waves. The axes show nondimensionalized wave number and frequency. The blue box indicates the long-wave regime. $n=0$ indicates the Rossby-gravity (Yanai) wave. Kelvin wave formally corresponds to $n=-1$. From Gill AE (1982) *Atmosphere-Ocean Dynamics*, 664pp. New York: Academic Press.

The meridional structure of the solutions of eqn [15] corresponding to the dispersion relation in [16] is described by Hermite functions:

$$\tilde{v} = \left(\sqrt{\pi}2^n n!\right)^{-1/2} H_n\left((\beta/c)^{1/2} y\right) \mathrm{e}^{-(\beta/2c)y^2} \quad [19]$$

where $H_n(Y)$ are Hermite polynomials ($n=0$, 1, 2, 3, …),

$$H_0 = 1;\ H_1 = 2Y;\ H_2 = 4Y^2 - 2;$$
$$H_3 = 8Y^3 - 12Y; H_4 = 16Y^4 - 48Y^2 + 12; \ldots, \quad [20]$$

and

$$Y = (\beta/c)^{1/2} y \quad [21]$$

These functions as defined in [19]–[21] are orthonormal.

The structure of Hermite functions, and hence of the meridional flow corresponding to different types of waves, is plotted in Figure 7. Hermite functions of odd numbers ($n=1$, 3, 5, …) are characterized by zero meridional flow at the equator. It can be shown that they create symmetric thermocline depth anomalies with respect to the equator (e.g., a first-order Rossby wave with $n=1$ has two equal maxima in the thermocline displacement on each side of the equator). Hermite functions of even numbers generate cross-equatorial flow and create thermocline displacement asymmetric with respect to the equator (i.e., with a maximum in the thermocline displacement on one side of the equator, and a minimum on the other).

It is Rossby waves of low odd numbers and Kelvin waves that usually dominate the solutions for large-scale tropical problems. This suggests that solving the equations can be greatly simplified by filtering out Poincare and short Rossby waves. Indeed, the long-wave approximation described earlier does exactly that. Such an approximation is equivalent to keeping only the waves that fall into the small box in Figure 6, as well as a remnant of the Yanai wave, and then linearizing the dispersion relations for small k. This makes long Rossby wave non-dispersive, each mode satisfying a simple dispersion relation with a fixed n:

$$\omega = -\frac{c}{2n+1}k, \quad n = 1, 2, 3, \ldots \quad [22]$$

Consequently, the phase speed of Rossby waves of different modes is $c/3$, $c/5$, $c/7$, etc. The phase speed of the first Rossby mode with $n=1$ is $c/3$, that is, one-third of the Kelvin wave speed. It takes a Kelvin wave approximately 2.5 months and a Rossby wave 7.5 months to cross the Pacific. The higher-order Rossby modes are much slower. The role of Kelvin and Rossby waves in ocean adjustment is described in the following sections.

Ocean Response to Brief Wind Perturbations

First, we will discuss the classical problem of ocean response to a brief relaxation of the easterly trade winds. These winds normally maintain a strong east–west thermocline slope along the equator

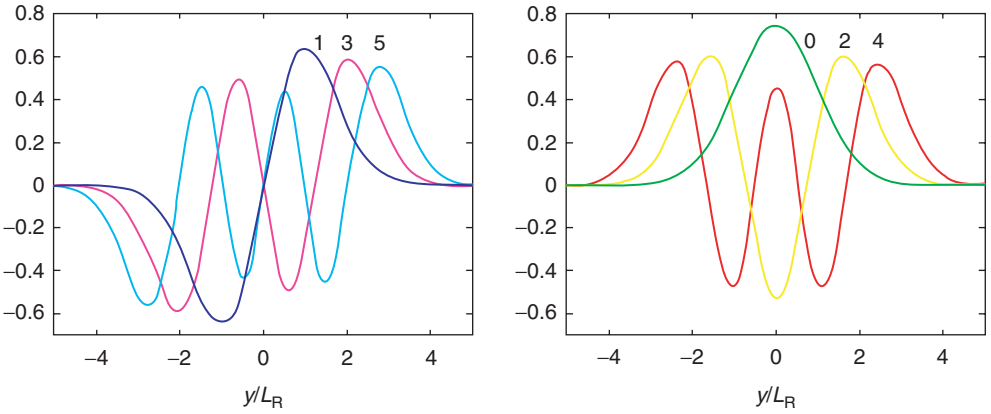

Figure 7 The meridional structure of Hermite functions corresponding to different equatorial modes (except for the Kelvin mode). The meridional velocity v is proportional to these functions. Left: Hermite functions of odd numbers ($n = 1, 3, 5, \ldots$) with no meridional flow crossing the equator. The flow is either converging or diverging away from the equator, which produces a symmetric structure (with respect to the equator) of the thermocline anomalies. Right: Hermite functions of even numbers ($n = 0, 2, 4, \ldots$) with nonzero cross-equatorial flow producing asymmetric thermocline anomalies.

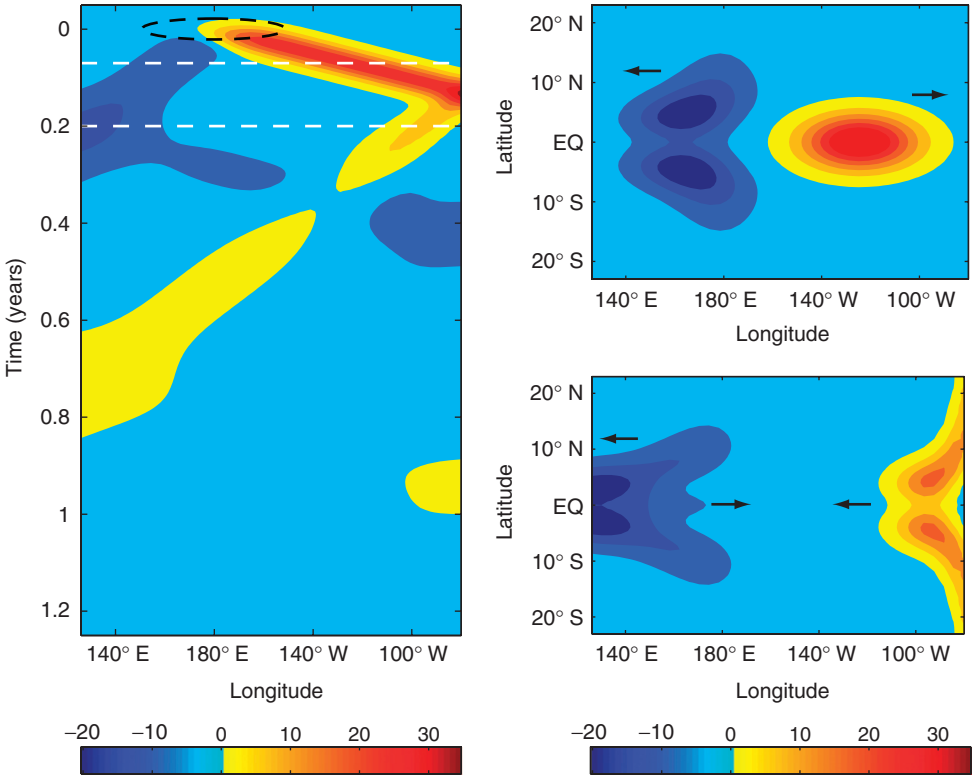

Figure 8 Ocean response to a brief westerly wind burst (WWB) occurring around time $t = 0$ in a shallow-water model of the Pacific. Left: a Hovmoller diagram of the thermocline depth anomalies along the equator (in meters). Note the propagation and reflection of Kelvin and Rossby waves (the signature of Rossby waves on the equator is usually weak and rarely seen in the observations). Right: the spatial structure of the anomalies at times indicated by the white dashed lines on the left-side panel. The arrows indicate the direction of wave propagation. The wind-stress perturbation is given by $\tau = \tau_{wwb} \exp[-(t/t_0)^2 - (x/L_x)^2 - (y/L_y)^2]$. Red corresponds to a deeper thermocline, blue to a shallower thermocline. The black dashed ellipse indicates the timing and longitudinal extent of the WWB.

and their changes therefore affect the ocean state. Westerly wind bursts (WWBs) that occur over the western tropical Pacific in the neighborhood of the dateline, lasting for a few weeks to a month, are examples of such occurrences. (Early theories treated El Niño as a simple response to a wind relaxation caused by a WWB. Arguably, WWBs may have contributed to the development of

El Niño in 1997, but similar wind events on other occasions failed to have such an effect.)

As compared to the timescales of ocean dynamics, these wind bursts are relatively short, so that ocean adjustment occurs largely when the burst has already ended. In general, the wind bursts have several effects on the ocean, including thermodynamic effects modifying heat and evaporation fluxes in the western tropical Pacific. The focus of this article is on the dynamic effects of the generation, propagation, and then boundary reflection of Kelvin and Rossby waves.

The results of calculations with a shallow-water model in the long-wave approximation are presented next, in which a WWB lasting ~ 3 weeks is applied at time $t = 0$ in the Pacific. The temporal and spatial structure of the burst is given by

$$\tau = \tau_{\mathrm{wwb}} \mathrm{e}^{-(t/t_0)^2 - (y/L_y)^2 - (x-x_0)^2/L_x^2} \qquad [23]$$

which is roughly consistent with the observations. The burst is centered at $x_0 = 180^\circ$ W; and $L_x = 10^\circ$; $L_y = 10^\circ$; $t_0 = 7$ days; $\tau_{\mathrm{wwb}} = 0.02\ \mathrm{N\ m^{-2}}$.

The WWB excites a downwelling Kelvin wave and an upwelling Rossby wave seen in the anomalies of the thermocline depth. Figure 8 shows a Hovmoller diagram and the spatial structure of these anomalies at two particular instances. The waves propagate with constant speeds, although in reality Kelvin waves should slow down in the eastern part of the basin where the thermocline shoals (since $c = (g'H)^{1/2}$). The smaller slope of the Kelvin wave path on the Hovmoller diagram corresponds to its higher phase speed, as compared to Rossby waves.

The spatial structure of the thermocline anomalies at two instances is shown on the right panel of Figure 8. The butterfly shape of the Rossby wave (meridionally symmetric, but not zonally) is due to the generation of slower, high-order Rossby waves that trail behind (higher-order Hermite functions extend farther away from the equator, Figure 7).

The waves reflect from the western and eastern boundaries (in the model the reflection coefficients were set at 0.9). When the initial upwelling Rossby wave reaches the western boundary, it reflects as an equatorial upwelling Kelvin wave. When the downwelling Kelvin wave reaches the eastern boundary, a

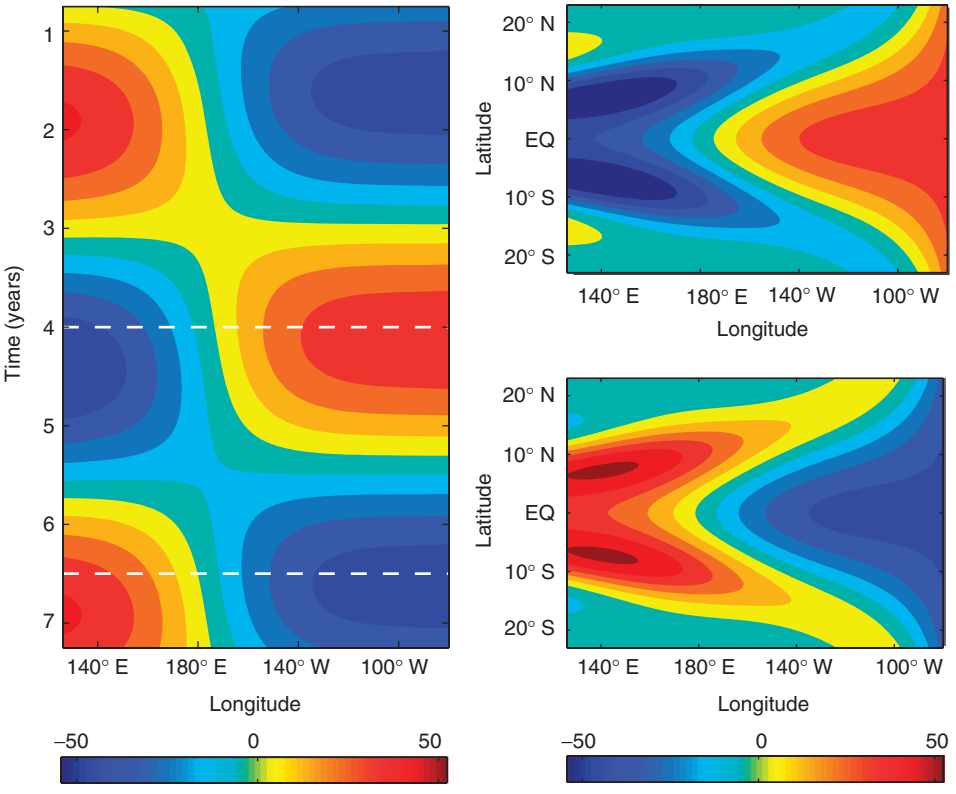

Figure 9 Ocean response to oscillatory winds in a shallow-water model. Left: a Hovmoller diagram of the thermocline depth anomalies along the equator. Note the different temporal scale as compared to Figure 8. Right: the spatial structure of the anomalies at times indicated by the dashed lines on the left-side panel. Red corresponds to a deeper thermocline, blue to a shallower thermocline. The wind-stress anomaly is calculated as $\tau = \tau_0 \sin(2\pi t/P)^* \exp[-(x/L_x)^2 - (y/L_y)^2]$; $P = 5$ years.

number of things occur. Part of the wave is reflected back along the equator as an equatorial downwelling Rossby wave. The remaining part travels north and south as coastal Kelvin waves, apparent in the lower right panel of Figure 8, which propagate along the west coast of the Americas away from the Tropics.

Ocean Response to Slowly Varying Winds

Ocean response to slowly varying periodic or quasi-periodic winds is quite different. The relevant zonal dynamical balance (with damping neglected) is

$$(u_t - \beta y v) + g' h_x = \tau^x / \rho D \qquad [24]$$

It is the balance between the east–west thermocline slope and the wind stress that dominates the equatorial strip. Off the equator, however, the local wind stress is not in balance with the thermocline slope as the Coriolis acceleration also becomes important.

The results of calculations with a shallow-water model in which a periodic sinusoidal forcing with the period P is imposed over the ocean are presented in Figure 9. The spatial and temporal structure of the forcing is given by

$$\tau = \tau_0 \sin(2\pi t/P) e^{-(y/L_y)^2 - (x-x_0)^2/L_x^2} \qquad [25]$$

where we choose $x_0 = 180^\circ$ W; $L_x = 40^\circ$; $L_y = 10^\circ$; and $\tau_0 = 0.02\,\mathrm{N\,m^{-2}}$; and $P = 5$ years. This roughly approximates to interannual wind stress anomalies associated with ENSO.

Figure 9 shows a Hovmoller diagram and the spatial structure of the ocean response at two particular instances. The thermocline response reveals slow forced anomalies propagating eastward along the equator. As discussed before, mathematically they can be obtained from a supposition of Kelvin and Rossby modes; however, the individual free waves are implicit and cannot be identified in the response. At the peaks of the anomalies, the spatial structure of the ocean response is characterized by

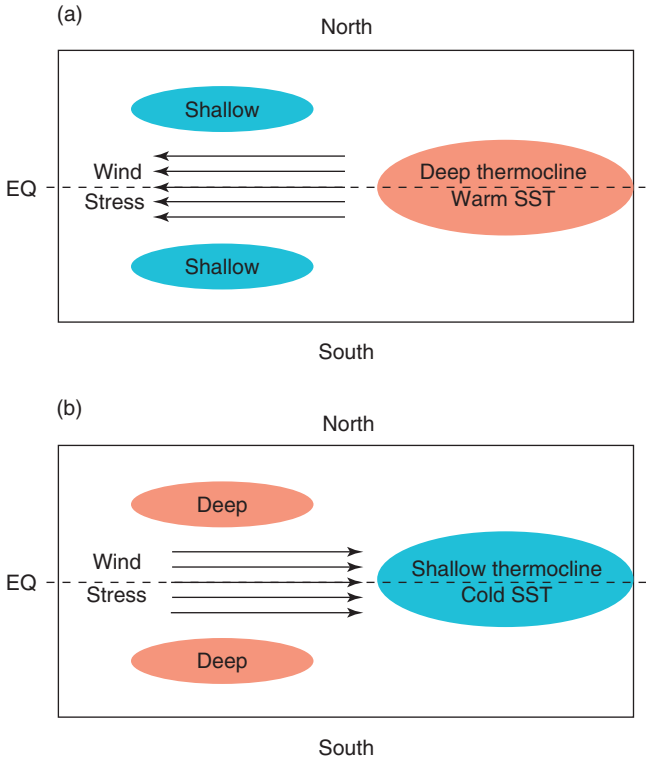

Figure 10 A schematic diagram that shows the spatial (longitude–latitude) structure of the coupled 'delayed oscillator' mode. Arrows indicate anomalous wind stresses, colored areas changes in thermocline depth. The sketch shows conditions during (a) El Niño and (b) La Niña. The off-equatorial anomalies are part of the ocean response to varying winds (cf. Figure 9). While the spatial structure of the mode resembles a pair of free Kelvin and Rossby waves, it is not so. The transition from (a) to (b) includes the shallow off-equatorial anomalies in thermocline depth slowly feeding back to the equator along the western boundary and then traveling eastward to reemerge in the eastern equatorial Pacific and to push the thermocline back to the surface. It may take, however, up to several years, instead of a few months, to move from (a) to (b). From Fedorov AV and and Philander SG (2001) A stability analysis of tropical ocean–atmosphere interactions: Bridging measurements and theory for El Niño. *Journal of Climate* 14(14): 3086–3101.

thermocline depression or elevation in the eastern equatorial Pacific (in a direct response to the winds) and off-equatorial anomalies of the opposite sign in the western equatorial Pacific.

Conceptual Models of ENSO Based on Ocean Dynamics

So far the equatorial processes have been considered strictly from the point of view of the ocean. In particular, we have shown that wind variations are able to excite different types of anomalies propagating on the thermocline – from free Kelvin and Rossby waves generated by episodic wind bursts to gradual changes induced by slowly varying winds. However, in the Tropics variations in the thermocline depth can affect SSTs and hence the winds, which gives rise to tropical ocean–atmosphere interactions.

The strength of the easterly trade winds (that maintain the thermocline slope in Figure 1) is roughly proportional to the east–west temperature

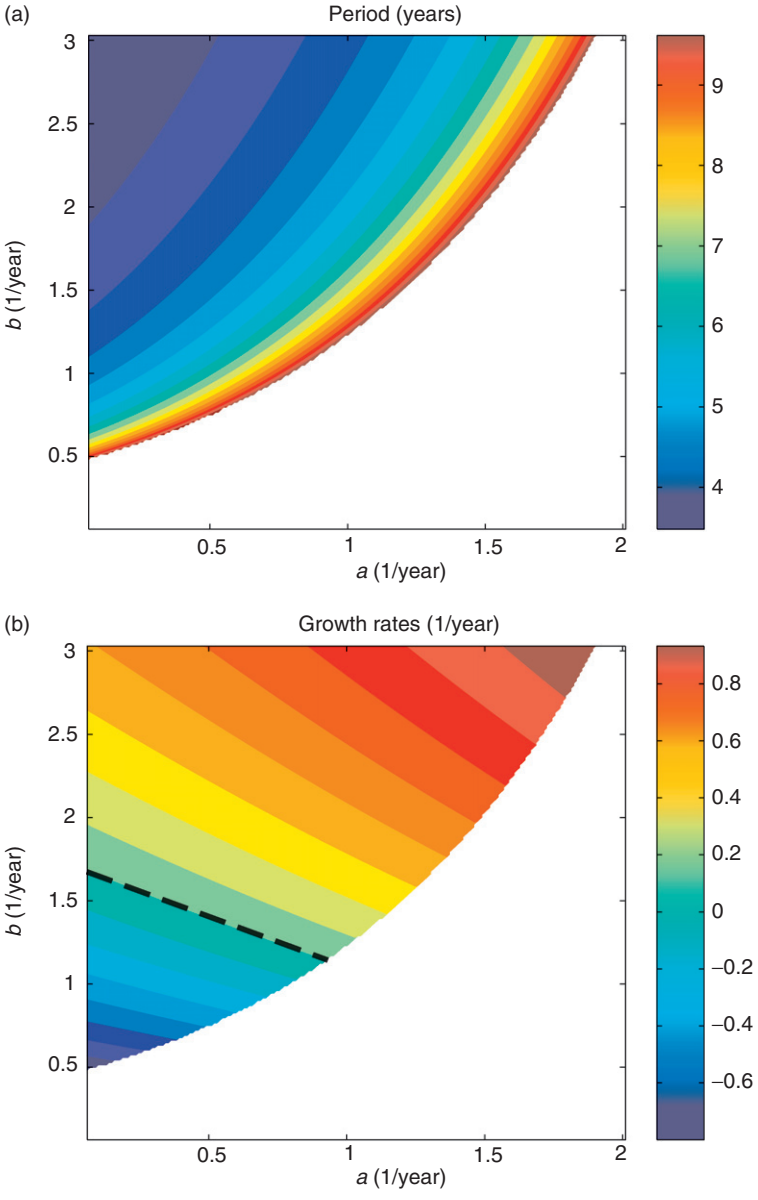

Figure 11 The period and the e-folding growth (decay) rates of the ENSO-like oscillation given by the delayed oscillator model $dT/dt = aT - bT(t-\Delta)$ as a function of a and b; for the delay $\Delta = 12$ months. The solutions of the model are searched for as $e^{\sigma t}$, where σ is a complex frequency. In the white area of the plot there are no oscillatory, but only exponentially growing or decaying solutions. At the border between the white and color areas the oscillation period goes to infinity, that is, $\mathrm{imag}(\sigma) = 0$. The dashed line in (b) indicates neutral stability. Note that the period of the oscillation can be much longer than the delay Δ used in the equation.

gradient along the equator. This implies a circular dependence: for instance, weaker easterly winds, during El Niño, result in a deeper thermocline in the eastern equatorial Pacific, weaker zonal SST gradient, and weaker winds. This is a strong positive feedback usually referred to as the Bjerknes feedback. On the other hand, the gradual oceanic response to changes in the winds (often referred to as 'ocean memory') provides a negative feedback and a potential mechanism for oscillatory behavior in the system. In fact, the ability of the ocean to undergo slow adjustment delayed with respect to wind variations and the Bjerknes feedback serve as a basis for one of the first conceptual models of ENSO – the delayed oscillator model.

Delayed Oscillator

Zonal wind fluctuations associated with ENSO occur mainly in the western equatorial Pacific and give rise to basin-wide vertical movements of the thermocline that affect SSTs mainly in the eastern equatorial Pacific. During El Niño, the thermocline in the east deepens resulting in the warming of surface waters. At the same time, the thermocline in the west shoals; the shoaling is most pronounced off the equator.

In this coupled mode, shown schematically in Figure 10, the response of the zonal winds to changes in SST is, for practical purposes, instantaneous, and this gives us the positive Bjerknes feedback described above. Ocean adjustment to changes in the winds, on the other hand, is delayed. The thermocline anomalies off the equator slowly feed back to the equator along the western boundary and then travel eastward, reemerging in the eastern equatorial Pacific, pushing the thermocline back to the surface, and cooling the SST. It may take up to a year or two for this to occur. This mode can therefore be called as a 'delayed oscillator' mode.

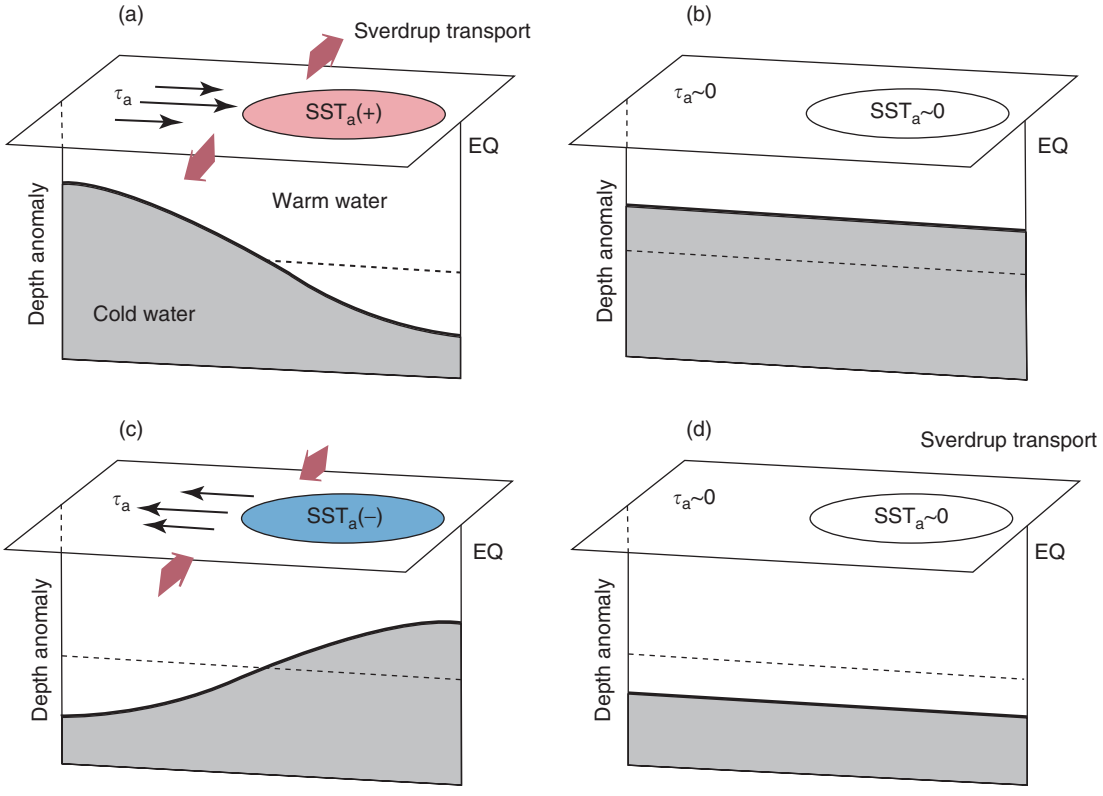

Figure 12 (a–d) A sketch showing the recharge-discharge mechanism of ENSO. All quantities are anomalies relative to the climatological mean. Depth anomaly is relative to the time mean state along the equator. Dashed line indicates zero anomaly; shallow anomalies are above the dashed line and deep anomalies are below the dashed line. Thin arrows and symbol τ_a represent the anomalous zonal wind stress; bold thick arrows represent the corresponding anomalous Sverdrup transports. SST_a is the sea surface temperature anomaly. Oscillation progresses from (a) to (b), (c), and (d) clockwise around the panels following the roman numerals; panel (a) represents El Niño conditions, panel (c) indicates La Niña conditions. Note similarities with Figure 10. Modified from Jin FF (1997) An equatorial ocean recharge paradigm for ENSO. 1. Conceptual model. *Journal of the Atmospheric Sciences* 54: 811–829 and Meinen CS and McPhaden MJ (2000) Observations of warm water volume changes in the equatorial Pacific and their relationship to El Niño and La Niña. *Journal of Climate* 13: 3551–3559.

An equation that captures the essence of this mode is

$$T_t = aT + bT(t - \Delta) \quad [26]$$

where T is temperature, a and b are constants, t is time, and Δ is a constant time lag. The first term on the right-hand side of the equation represents the positive feedbacks between the ocean and atmosphere (including the Bjerknes feedback). It is the presence of the second term that describes the delayed response of the ocean that permits oscillations (the physical meaning of the delay Δ is the time needed for an off-equatorial anomaly in the western Pacific to converge to the equator and then travel to the eastern Pacific).

The period of the simulated oscillation depends on the values of a, b, and Δ. Solutions of eqn [26] proportional to $e^{\sigma t}$ give a transcendental algebraic equation for the complex frequency σ

$$\sigma = a - be^{-\sigma t} \quad [27]$$

where

$$\sigma = \sigma_r + i\sigma_i \quad [28]$$

The solutions of eqn [27] are shown in Figure 11 for $\Delta = 1$ year and different combinations of a and b.

Even though the term 'delayed oscillator' appears frequently in the literature, there is some confusion concerning the roles of Kelvin and Rossby waves, which some people seem to regard as the salient features of the delayed oscillator. The individual waves are explicitly evident when the winds change abruptly (Figure 6), but those waves are implicit when gradually varying winds excite a host of waves, all superimposed (Figure 7). For the purpose of deriving the delayed-oscillator equation, for instance, observations of explicit Kelvin (and for that matter individual Rossby) waves are irrelevant. The gradual eastward movement of warm water in Figure 7 (left panel) is the forced response of the ocean and cannot be a wave that satisfies the unforced equations of motion.

Recharge Oscillator

The delayed oscillator gave rise to many other conceptual models based on one or another type of the delayed-action equation (the Western Pacific, Advection, Unified oscillators, just to name a few, each emphasizing particular mechanisms involved in ENSO). A somewhat different approach was used by Jin in 1997 who took advantage of the fact that free Kelvin waves cross the Pacific very quickly, which allowed him to eliminate Kelvin waves from

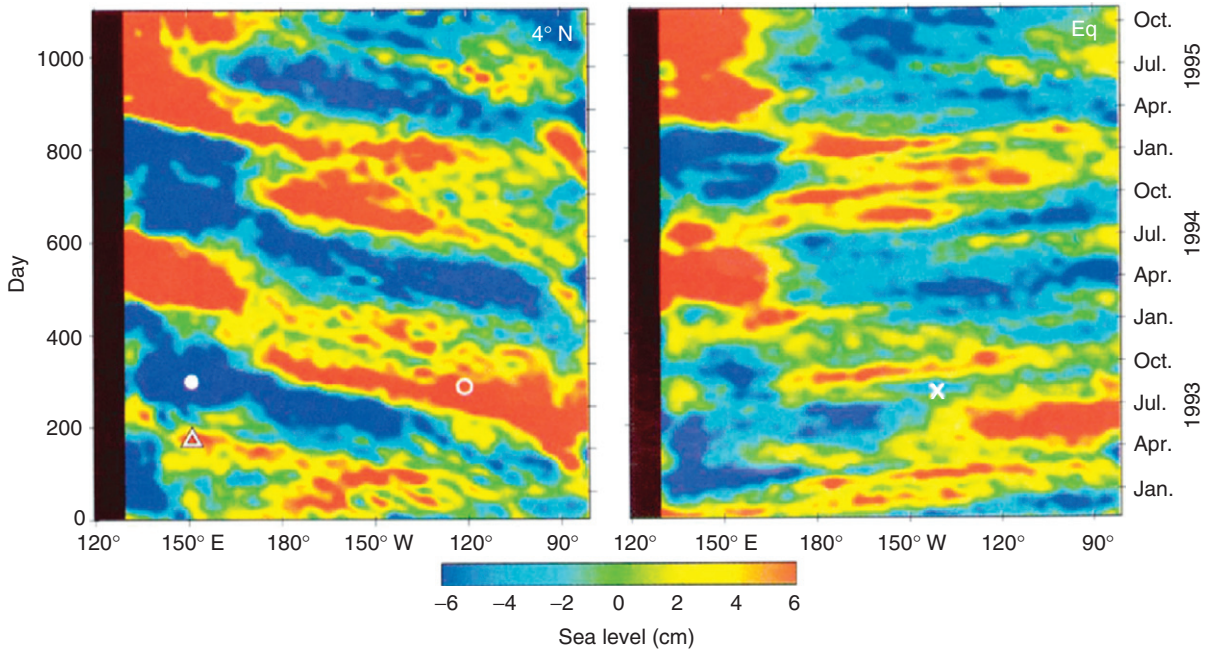

Figure 13 Observations of Rossby (left) and Kelvin (right) waves. Time-longitude sections of filtered sea level variations in the Pacific Ocean along 4° N and along the equator are shown. A section along 4° S would be similar to the 4° N section. The symbols (x, triangle, and circles) correspond to the times and locations of the matching symbols in Figure 14. Note that time runs from bottom to top. Obtained from TOPEX/POSEIDON satellite data; from Chelton DB and Schlax MG (1996) Global observations of oceanic Rossby Waves. *Science* 272(5259): 234–238.

consideration and derive the recharge oscillator model.

The recharge oscillator theory is now one of the commonly used paradigms for ENSO. It relies on a phase lag between the zonally averaged thermocline depth anomaly and changes in the eastern Pacific SST. Consider first a 'recharged' ocean state (Figure 12(d)) with a deeper than normal thermocline across the tropical Pacific. Such a state is conducive to the development of El Niño as the deep thermocline inhibits the upwelling of cold water in the east. As El Niño develops (Figure 12(a)), the reduced zonal trade winds lead to an anomalous Sverdrup transport out of the equatorial region. The ocean response involves a superposition of many equatorial waves resulting in a shallower than normal equatorial thermocline and the termination of El Niño (Figure 12(b)).

The state with a shallower mean thermocline (the 'discharged' state) is usually followed by a La Niña event (Figure 12(c)). During and after La Niña the enhanced trade winds generate an equatorward flow, deepening the equatorial thermocline and eventually 'recharging' the ocean (Figure 12(d)). This completes the cycle and makes the ocean ready for the next El Niño event.

Observations of Kelvin and Rossby Waves, and El Niño

Thirty years ago very little was known about tropical processes, but today an impressive array of instruments, the TAO array, now monitors the equatorial Pacific continuously. It is now possible to follow, as they happen, the major changes in the circulation of the tropical Pacific Ocean that accompany the alternate warming and cooling of the surface waters of the eastern equatorial Pacific associated with El Niño and La Niña. Satellite-borne radiometers and

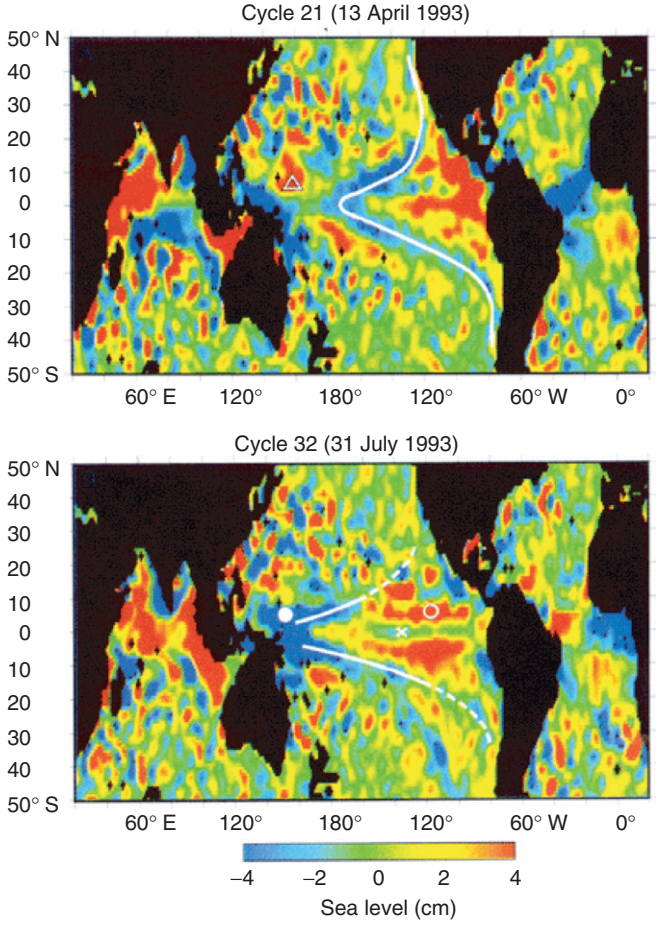

Figure 14 Observations of Rossby waves: global maps of filtered sea level variations on 13 April 1993 and $3\frac{1}{2}$ months later on 31 July. White lines indicate the wave trough. The time evolution of the equatorial Kelvin wave trough (x), the Rossby wave crest (open triangle and open circle), and the Rossby wave trough (solid circle) can be traced from the matching symbols in Figure 13. Obtained from TOPEX/POSEIDON satellite data, from Chelton and Schlax (1996).

altimeters measure ocean temperature and sea level height almost in real time, providing information on slow (interannual) changes in the ocean thermal structure as well as frequent glimpses of swift wave propagation.

Figures 13 and 14 show the propagation of fast Kelvin and Rossby waves in the Pacific as seen in the satellite altimeter measurements of the sea level height. The speed of propagation of Kelvin waves agrees relatively well with the predictions from the theory ($\sim 2.7\,\mathrm{m\,s^{-1}}$). The speed of the first-mode Rossby waves, however, is estimated from the observation to be 0.5–0.6 $\mathrm{m\,s^{-1}}$, which is somewhat lower than expected, that is, 0.9 $\mathrm{m\,s^{-1}}$. This appears to be in part due to the influence of the mean zonal currents.

Estimated variations of the thermocline depth associated with the small changes in the sea level in Figure 13 are in the range of ± 5 m (stronger Kelvin waves may lead to variation up to ± 20 m). Note that the observed 'Rossby wave' in Figure 14 is actually a composition of Rossby waves of different orders; higher-order waves travel much slower. The waves are forced by high-frequency wind perturbations, even though it seems likely that annual changes in the zonal winds may have also contributed to the forcing of Rossby waves.

As mentioned above, there is a clear distinction between free Kelvin waves and slow wave-like anomalies associated with ENSO. This is further emphasized by the measurements in Figure 15 that contain evidence of freely propagating Kelvin waves (dashed lines in the left panel) but clearly show them to be separate from the far more gradual eastward movement of warm water associated with the onset of El Niño of 1997 (a dashed line in the right panel). This slow movement of warm water is the forced response of the ocean and clearly not a wave that could satisfy the unforced equations of motion. The characteristic timescale of ENSO cycle, several years, is so long that low-pass filtering is required to isolate its structure. That filtering eliminates individual Kelvin waves in the right-side panel of the figure. Whether the high- and low-frequency components of

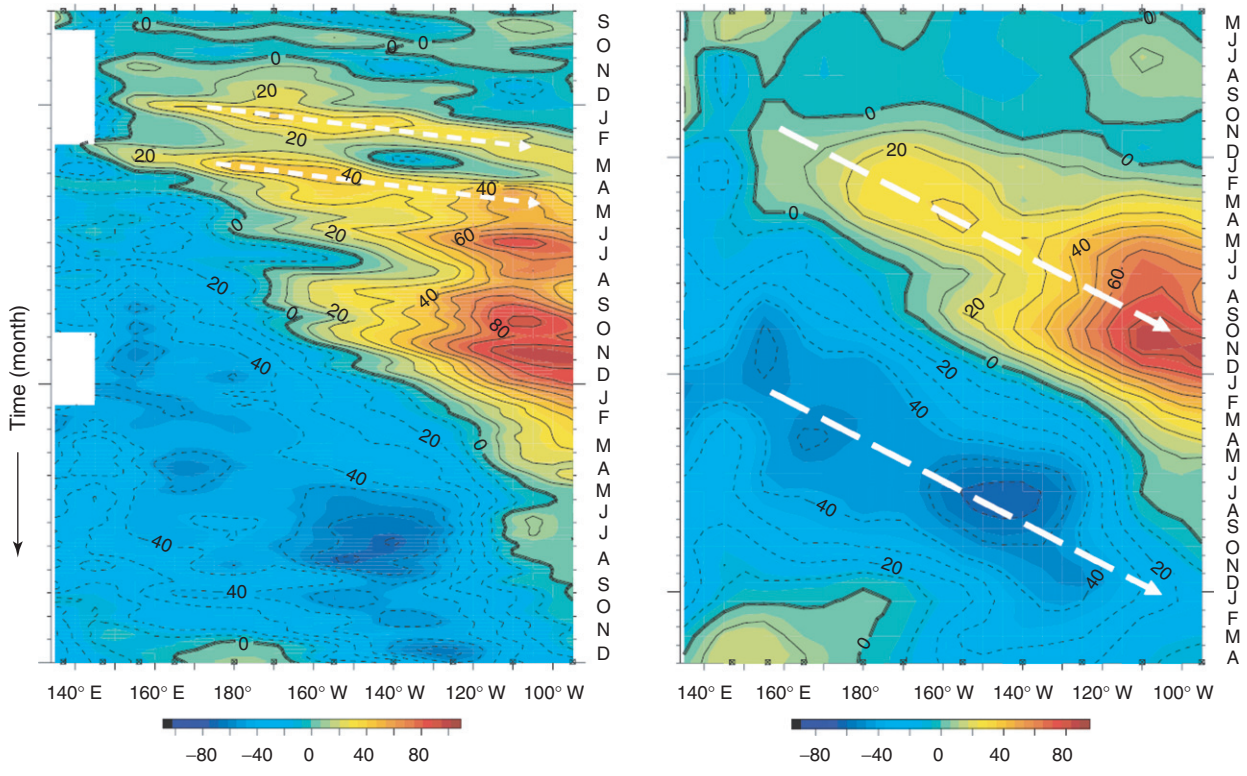

Figure 15 Observations of Kelvin waves and El Niño from the TAO array. Anomalies with respect to the long-term average of the depth of the 20 °C-degree isotherm are shown before and after the development of El Niño of 1997. Left: 5-day averages; the time axis starts in September 1996. Right: monthly averages; the time axis starts in May 1996 (cf. Figures 8 and 9). The dashed lines in the left-side panel correspond to Kelvin waves excited by brief WWBs and rapidly traveling across the Pacific. The dashed lines in the right-side panel show the slow eastward progression of warm and cold temperature anomalies associated with El Niño followed by a La Niña. The monthly averaging effectively filters out fast Kelvin waves from the picture leaving only gradual interannual changes. It has been argued that the Kelvin waves may have contributed to the exceptional strength of El Niño in 1997–98.

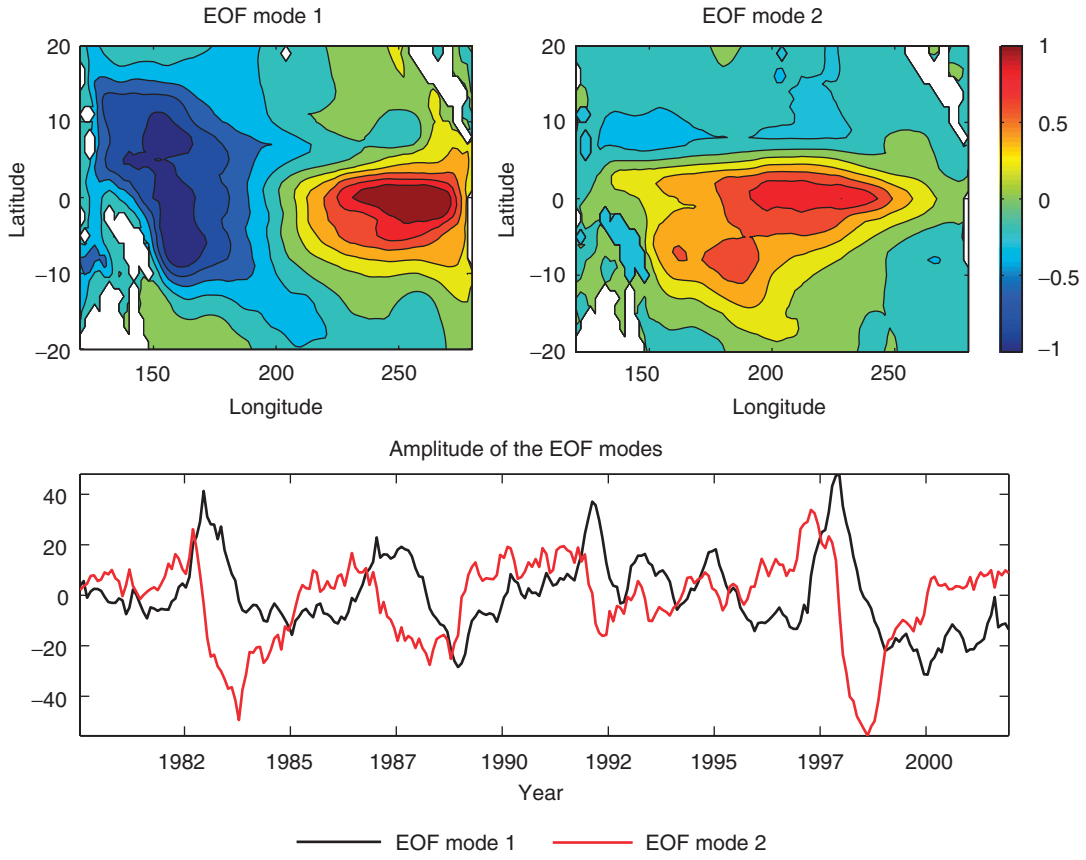

Figure 16 The first two empirical orthogonal functions (EOFs) of the thermocline depth variations (approximated as the 20 °C-degree isotherm depth) in the tropical Pacific. The upper panels denote spatial structure of the modes (nondimensionalized), while the lower panel shows mode amplitudes as a function of time (cf. **Figure 12**). The data are from hydrographic measurements combined with moored temperature measurements from the tropical atmosphere and ocean (TAO) array, prepared by Neville Smith's group at the Australian Bureau of Meteorology Research Centre (BMRC). Adapted from Meinen CS and McPhaden MJ (2000) Observations of warm water volume changes in the equatorial Pacific and their relationship to El Niño and La Niña. *Journal of Climate* 13: 3551–3559.

the signal can interact remains to be seen, even though it has been argued that the Kelvin waves in Figure 15 may have contributed to the exceptional strength of El Niño of 1997–98.

The observations also provide confirmation of the recharge oscillator mechanism, which can be demonstrated, for example, by calculating the empirical orthogonal functions (EOFs) of the thermocline depth (Figure 16). The first EOF (the left top panel) shows the spatial structure associated with changes in the slope of the thermocline, and its temporal variations are well correlated with SST fluctuations in the eastern equatorial Pacific, or the ENSO signal. The second EOF shows changes in the mean thermocline depth, that is, the 'recharge' of the equatorial thermocline. The time series for each EOF in the bottom panel of Figure 16 indicate that the second EOF (the thermocline recharge) leads the first EOF (a proxy for El Niño) by approximately 7 months.

Summary

Early explanations of El Niño that relied on the straightforward generation of free Kelvin and Rossby waves by a WWB have been superseded. Modern theories consider ENSO in terms of a slow oceanic adjustment which occurs as a sum of continuously forced equatorial waves. The concept of 'ocean memory' based on the delayed ocean response to varying winds has become one of the cornerstones for explaining ENSO cyclicity. It is significant that although from the point of view of the ocean a superposition of forced equatorial waves is a direct response to the winds, from the point of view of the coupled ocean–atmosphere system it is a part of a natural mode of oscillation made possible by ocean–atmosphere interactions.

Despite considerable observational and theoretical advances over the past few decades many issues are still being debated and each El Niño still brings

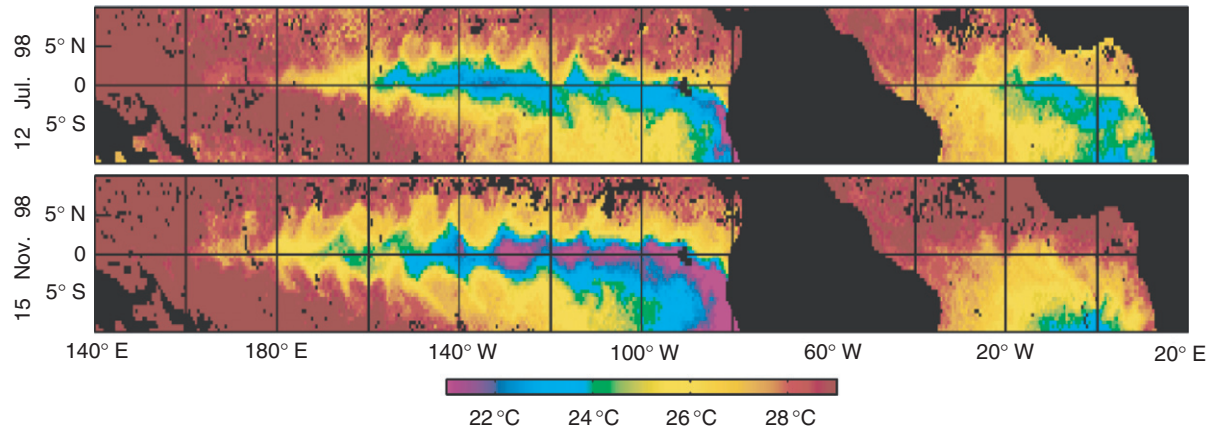

Figure 17 Tropical instability waves (TIWs): 3-day composite-average maps from satellite microwave SST observations for the periods 11–13 July 1998 (upper) and 14–16 November 1998 (lower). Black areas represent land or rain contamination. The waves propagate westward at approximately 0.5 m s^{-1}. From Chelton DB, Wentz J, Gentemann CL, de Szoeka RA, and Schlax MG (2000) Satellite microwave SST observations of trans-equatorial tropical instability waves. *Geophysical Research Letters* 27(9): 1239–1242.

surprises. The prolonged persistence of warm conditions in the early 1990s was as unexpected as the exceptional intensity of El Niño in 1982 and again in 1997. Prediction of El Niño also remains problematic. Not uncommonly, when a strong Kelvin wave crosses the Pacific and leaves a transient warming of 1–2 °C in the eastern part of the basin, a question arises whether this might be a beginning of the next El Niño. To what degree, random transient disturbances influence ENSO dynamics remains unclear.

Many theoretical and numerical studies argue that high-frequency atmospheric disturbances, such as WWBs that excite Kelvin waves, can potentially interfere with ENSO and can cause significant fluctuations in its period, amplitude, and phase. Other studies, however, insist that external to the system atmospheric 'noise' has only a marginal impact on ENSO. To resolve this issue we need to know how unstable the coupled system is. If it is strongly damped, there is no connection between separate warm events, and strong wind bursts are needed to start El Niño. If the system is sufficiently unstable then a self-sustained oscillation is possible. The truth is probably somewhere in between – the coupled system may be close to neutral stability, perhaps weakly damped. Random atmospheric disturbances are necessary to sustain a quasi-periodic, albeit irregular oscillation.

Another source of random perturbations that affects both the mean state and interannual climate variations is the tropical instability waves (TIWs) typically observed in the high-resolution snapshots of tropical SSTs (Figure 17). These waves, propagating westward with typical phase speed of roughly 0.5 m s^{-1}, are excited by instabilities of the zonal equatorial currents with strong vertical and horizontal shear. The wave dynamical structure corresponds to that of cyclonic and anticyclonic eddies having maximum velocities near the ocean surface and penetrating into the ocean by a few hundred meters. The waves can affect the temperature of the equatorial cold tongue, and the properties of ENSO, by modulating meridional heat transport from the equatorial Pacific. Overall, the role of the TIWs remains a subject of intensive research which includes the effect of these waves on the coupling between the wind stress and SSTs and the interaction between the TIWs and Rossby waves.

See also

El Niño Southern Oscillation (ENSO). El Niño Southern Oscillation (ENSO) Models. Pacific Ocean Equatorial Currents.

Further Reading

Battisti DS (1988) The dynamics and thermodynamics of a warming event in a coupled tropical atmosphere/ocean model. *Journal of Atmospheric Sciences* 45: 2889–2919.

Chang PT, Yamagata P, Schopf SK, *et al.* (2006) Climate fluctuations of tropical coupled system – the role of ocean dynamics. *Journal of Climate* 19(20): 5122–5174.

Chelton DB and Schlax MG (1996) Global observations of oceanic Rossby waves. *Science* 272(5259): 234–238.

Chelton DB, Schlax MG, Lyman JM, and Johnson GC (2003) Equatorially trapped Rossby waves in the presence of meridionally sheared baroclinic flow in the Pacific Ocean. *Progress in Oceanography* 56: 323–380.

Chelton DB, Wentz J, Gentemann CL, de Szoeka RA, and Schlax MG (2000) Satellite microwave SST observations of trans-equatorial tropical instability waves. *Geophysical Research Letters* 27(9): 1239–1242.

Fedorov AV and Philander SG (2000) Is El Niño changing? *Science* 288: 1997–2002.

Fedorov AV and Philander SG (2001) A stability analysis of tropical ocean–atmosphere interactions: Bridging measurements and theory for El Niño. *Journal of Climate* 14(14): 3086–3101.

Gill AE (1982) *Atmosphere-Ocean Dynamics*, 664p. New York: Academic Press.

Jin FF (1997) An equatorial ocean recharge paradigm for ENSO. 1. Conceptual model. *Journal of the Atmospheric Sciences* 54: 811–829.

Kessler WS (2005) Intraseasonal variability in the oceans. In: Lau WKM and Waliser DE (eds.) *Intraseasonal variability of the Atmosphere-Ocean System*, pp. 175–222. Chichester: Praxis Publishing.

Levitus S and Boyer T (1994) *World Ocean Atlas 1994, Vol. 4: Temperature NOAA Atlas NESDIS4*. Washington, DC: US Government Printing Office.

McPhaden MJ (1999) Genesis and evolution of the 1997–98 El Niño. *Science* 283: 950–954.

Meinen CS and McPhaden MJ (2000) Observations of warm water volume changes in the equatorial Pacific and their relationship to El Niño and La Niña. *Journal of Climate* 13: 3551–3559.

Philander G (1990) *El Niño, La Niña, and the Southern Oscillation. International Geophysics Series*, 293p. New York: Academic Press.

Schopf PS and Suarez MJ (1988) Vacillations in a coupled ocean atmosphere model. *Journal of the Atmospheric Sciences* 45: 549–566.

Wang C, Xie SP, and Carton JA (2004) Earth's climate: The ocean–atmosphere interaction. *Geophysical Monograph 147, American Geophysical Union*, 405p.

Zebiak SE and Cane MA (1987) A model El Niño-southern oscillation. *Monthly Weather Review* 115(10): 2262–2278.

Relevant Website

http://www.pmel.noaa.gov
– Tropical Atmosphere Ocean Project, NOAA.